Scratch hardness as a quasi-intrinsic parameter to measure the scratch resistance of polymers

Luca Andena*, Giulia Chiarot
Dipartimento di Chimica, Materiali e Ingegneria Chimica "Giulio Natta", Politecnico di Milano

Abstract

In this work four different polymers (acrylonitrile-butadiene-styrene, high-impact polystyrene, rubber-toughened polybutylene terephthalate, linear low-density polyethylene) were characterized in terms of their bulk (modulus and yield stress) and surface (scratch hardness) mechanical properties. The intrinsic time-dependence of the materials was addressed by performing DMA and compression tests at varying testing speed/frequency, exploiting time-temperature superposition and Eyring's model to obtain data at strain rates compatible with scratch experiments. The latter were performed by applying different loading histories (constant depth or load) and indenters. Scratch hardness was determined using Pelletier's model; it was demonstrated that such a parameter provides a reliable and almost intrinsic (i.e. loading history independent) evaluation of scratch resistance, seen as the resistance the material opposes to indenter penetration. Its relation with other aspects of the scratch phenomenon (in particular deformation recovery) was also explored, accounting for the specific deformation regime imposed by the indenter (transitioning from elastic to predominantly plastic).

Keywords
Polymers, scratch testing, hardness, viscoelasticity

1. Introduction

The study of scratch behaviour of ductile polymers is of great importance for all those applications requiring a high surface quality, such as in the automotive sector, but also data storage and optical industries. Scratch response is commonly analysed by means of a scratch test, which consists in sliding an indenter with a specific geometry on the sample surface, under controlled testing conditions [1-9]. Such a test can reproduce the elementary process responsible for abrasive wear of relatively soft materials (such as polymers) when in contact with hard asperities, representing individual particles or the rough surface of a harder body the material is in contact with. The main problem related to the description of this process is, despite its highly simplified nature, the difficulty in accounting for all the parameters that influence the final response of the material. Moreover, when dealing with viscoelastic-viscoplastic materials, such as polymers, also temperature and strain rate dependence affect the final damage appearance [10-16]. Several approaches have been proposed in the scientific literature to characterize scratch resistance, widely different in their scope and applicability.
The most direct way of evaluating scratch damage is to assess how the optical properties change as a consequence of scratching [2,17-25]. However, scratch visibility is influenced by a huge number of different variables, only partially related to the material: colour, roughness, type and geometry of lighting, angle of observation. Moreover, the link between objective measurements (as performed by a camera system) and subjective human perception is still not consolidated. While this type of analysis is of paramount importance in view of many applications, it is quite

challenging to follow this route and obtain a determination of the intrinsic material scratch resistance.
Traditionally, scratch maps have been used as an alternative route to describe the scratch behaviour of materials, and polymers in particular [6-7,26-27]. While they represent an effective method to highlight the effect of variables such as attack angle, load, speed or temperature on the relevant scratching mechanisms (e.g. ductile ploughing or brittle machining), again they cannot easily provide quantitative evidence of the performance exhibited by different materials. In a similar way, studies focused on post-scratch analysis of the residual scratch grooves [21,28-30], conducted using a variety of microscopy, diffractometry or spectroscopy techniques, can help in identifying the ongoing mechanisms. They can help to explain why a given material performs in a certain way; however, they do not offer a true measurement of the scratch resistance.
So far, the best attempt at providing this kind of quantitative evaluation is given by the determination of scratch hardness, H_S, defined as the ratio between the normal load and the projected contact area, measured from the residual scratch groove left on the surface by the indenter. It is clear that this definition is related to the notion of indentation hardness, as given by Brinell or Vickers hardness measurements, and is consistent with standards such as ASTM G171 [31]. However, its application could be questionable considering the large amount of recovery exhibited by polymeric material (the hardness of a rubber could be infinite!). In several studies, H_S is instead evaluated considering the contact area during the scratching process [6,10,13,15-16,27,32-34]. While in principle both definitions are valid, each one features its own advantages and disadvantages. The measurement of geometrical characteristics of the residual scratch grooves is clearly considerably easier than trying to evaluate the contact area during their formation, something which can be done only via modelling [5,9,12-13,23,35] and/or using a scratch tester equipped with *in-situ* observation (and limiting the analysis to transparent materials) [10,13,28,36]. The modelling step introduces the need to characterize the mechanical behaviour of the materials of interest, with additional effort (in particular for viscoelastic materials) and uncertainties; however, it allows to establish a correlation between scratch hardness and the effective contact pressure developed between the indenter and the scratched surface, and eventually with the material bulk mechanical properties [15-17]. Scratch hardness measured in such a way makes scratch testing a powerful surface probing technique, applicable to the study of degradation phenomena [37-38] or to the optimization of the composition of materials used for tribological applications [39-40].
Within this framework, the aim of the present paper is to validate a scratch-hardness based approach for the characterization of ductile engineering polymers, exploring the limits within such a parameter can be considered an intrinsic material property. For this purpose, a set of different materials is considered, with scratch tests performed using different indenters and loading conditions. The Pelletier's model [13] has been chosen to calculate scratch hardness from the experimental data, with a thorough characterization of the mechanical properties required by the model evaluated according to the viscoelastic nature of the materials under investigation.

2. Experimental

2.1. Materials

The range of materials investigated included four different polymers, object of a previous study dealing with the determination of their fracture resistance using a J-integral approach [41].
Two of them, an acrylonitrile-butadiene-styrene copolymer (ABS) and a high-impact polystyrene blend (HIPS), possess an amorphous structure; conversely, the other two – a rubber-toughened polybutylene terephthalate (RT-PBT) and a linear low-density polyethylene

(LLDPE) – are semicrystalline. Materials had originally been supplied by Versalis SpA (Mantova, Italy), with the exception of RT-PBT which had been provided by Radici Novacips SpA (Villa d'Ogna, Bergamo, Italy), and includes about 20% weight of rubber.
Material processing occurred via injection moulding. Tests were performed on dumbbell tensile samples, having a gauge length of 80 mm and a cross-section area of 10x4 mm^2; only in the case of LLDPE rectangular sheets were machined out of 5 mm thick injection moulded plates. The actual manufacturing details, together with basic mechanical properties also reported in [41], are listed in Table 1.

Table 1. Supplied form and basic mechanical properties of the investigated materials [41]

Material	Supplied form	Modulus, E	Yield stress, σ_y
		MPa	MPa
HIPS	Injection-moulded dumbbells	1760	18
ABS	Injection-moulded dumbbells	2300	46
RT-PBT	Injection-moulded dumbbells	1450	31
LLDPE	Injection-moulded plates	250	8

2.2. Methods

All the tests were performed at a temperature of 25°C, with the exception of DMA for which several temperatures were considered. At least three replicates for each test/condition were carried out.

2.2.1. Dynamic Mechanical Analysis (DMA)

Elastic modulus (E) measurements, required for the application of Pelletier's model, were obtained by means of a dynamic three-point bending test, performed with a TA Rheometric Series RSA III instrument. In particular, the value of the storage modulus, E' was considered, in view of the very small values of the loss angle obtained during the analysis (justifying the assumption that $E \approx E'$).
Specimen dimensions were 45x10x4 mm, except from LLDPE, whose samples measured 45x5x5 mm, since the slab thickness from which strips were cut was equal to 5 mm; in all the cases the span was 40 mm.
Measurements were performed with frequency (f) sweeps in the range between 0.1 and 10 Hz, with a constant maximum strain amplitude ε of 0.01%. The resulting effective strain rate, estimated for the region farther from the bending neutral axis, was simply taken as:

$$\dot{\varepsilon} = f \cdot \varepsilon \tag{1}$$

Tests were conducted at several (constant) temperatures in the range between -35°C and +25°C, using liquid nitrogen as a cooling agent and waiting a few minutes at each temperature to allow thermal equilibrium to be reached in the whole sample.

2.2.2. Quasi-static Compression

Tests were carried out using an Instron 1185R5800 dynamometer fitted with compression plates at constant crosshead speeds of 0.001, 0.01 and 0.1 mm/min; these values, divided by the initial sample height, directly provide the strain rate imposed during the tests.
Prismatic specimens with a square 4x4 mm^2 cross-section (5x5 mm^2 in the case of LLDPE) and height equal to twice the square side were cut from the DMA samples; to this purpose a CEAST

Notchvis machine, equipped with a razor blade, was employed. Details of the cutting technique used can be found in [43-46]; in this case, notches were run through the whole thickness of the specimens to obtain the desired length.
To reduce friction between the test specimen and the plates, thus limiting barrelling of the test specimens, a 15 μm thick polytetrafluoroethylene film was put between the sample faces and the metal plates. The displacement between the two plates was measured using a strain-gage extensometer.
The maximum of the stress-strain curves was taken as the yield stress value for ABS. For the other three materials, for which such a maximum was not apparent, the yield stress was taken as the intersection of two straight lines fitted through the initial and post-yield region of the stress vs. strain curves, as shown in Figure 1.

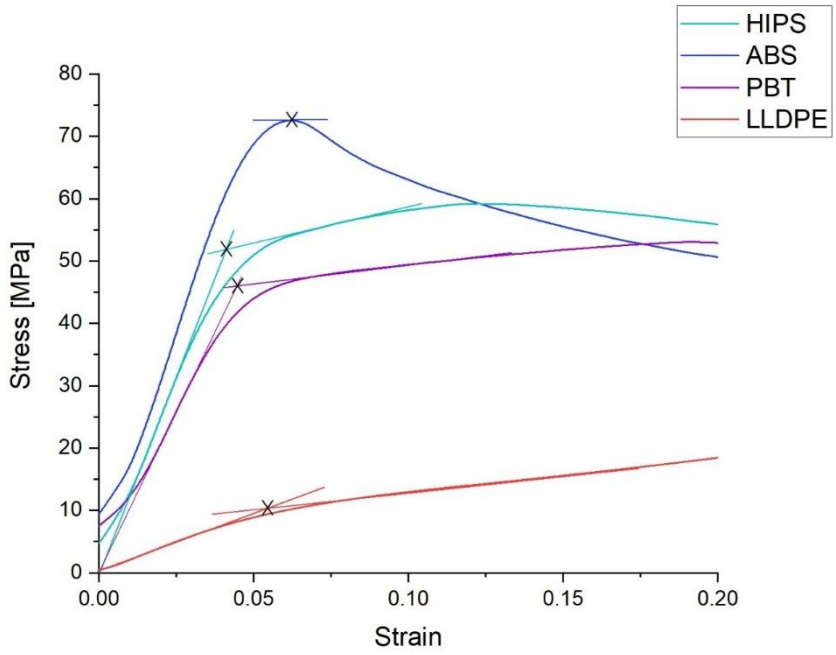

Figure 1. Stress-strain compression curves for the investigated materials, in which a graphical representation of the procedure used for the evaluation of the yield stress is given (maximum for ABS, intersection of bi-linear fit for the others). Toe correction was performed by horizontally shifting the curves, in such a way that a linear fitting of the initial, elastic part crosses the axis origin.

2.2.3. Microscratch

Scratch tests were performed on the grip parts of the dumbbell specimens in the case of HIPS and ABS, and on the central part (the only available one) for PBT. For what concerns LLDPE, a 60x30x5 mm strip was cut from the injection moulded plate. Before running the tests, all the samples were cleaned with alcohol in order to remove dirt and residuals of the cutting operations.
A CSM/Anton Paar Microscratch Tester was used with two different sphero-conical indenters, both having spherical diamond tips with radii of 200 μm, but differing in terms of their apex angle (120° and 90°). All tests were conducted applying a constant normal load, F_N, set to match a predefined value (in the range between 0.83 and 10 N) or adjusted to result in the same penetration depth (P_d) for all materials, equal to 40 μm; the latter, constant depth condition already proposed in [15] was explored only with the 120° indenter.
Pre- and post-scans performed at 30 mN normal load were performed to measure the initial profile (against which both P_d and R_d were evaluated) and the residual depth (R_d) of the scratch groove. Four values of the sliding velocity, v, were investigated for each material (0.5, 5, 50 and 250 mm/min) during the constant penetration depth tests, while those at varying loads were conducted at the single speed of 50 mm/min. The scratch length was 4 mm for all tests, except

for those at 0.5 mm in which the length was limited to 3 mm to reduce testing times. The acquisition rate was set between 0.5 and 30 Hz (the maximum value provided by the instrument), depending on the sliding speed, to ensure that a sufficient number of data points (> 25) was available for each scratch made.
Based on the analysis of Bucaille [42], the effective strain rate $\dot{\varepsilon}$ associated to the scratching process was taken as:

$$\dot{\varepsilon} \approx \frac{v}{P_d} \tag{2}$$

3. Theoretical background

3.1. Pelletier's model

With the aim of evaluating the scratch hardness of the selected materials, the Pelletier model [13] was exploited to calculate the contact area, according to the established definition of H_S:

$$H_S = \frac{F_N}{A} \tag{3}$$

with F_N being the applied normal load, and A the calculated contact area.
The model allows the determination of A from the experimental measurement of the penetration depth, P_d, and the rheological factor, X:

$$X = \frac{E}{\sigma_y} tan\ \beta \tag{4}$$

X depends on the mechanical properties of the material, namely the elastic modulus, E, and the yield stress, σ_y, and also on the indenter geometry via the attack angle, β. The latter has values of 30° and 45° for indenters having apex angles of 120° and 90°, respectively.
As a consequence of scratching, ductile materials such as the ones presently investigated deform elasto-plastically with the accumulation of material in front and to the sides of the indenter (pile-ups). The shape ratio, c^2, defines the ratio between the true contact depth, C_d, which includes the contribution of pile-up formation in front of the indenter, and the measured penetration depth, P_d:

$$c^2 = \frac{C_d}{P_d} \tag{5}$$

According to the Bucaille's [35] analysis, in the range of interest for the materials under investigation, the following empirical relationship between c^2 and X holds:

$$c^2 = 0.25339\ ln\ X\ + 0.5017 \tag{6}$$

(Visco)elastic recovery behind the indenter can be described with the parameter, α, defined as the angle between the direction perpendicular to the scratch and the last point of contact between the material and the rear part of the indenter. For an ideally plastic contact, $\alpha = 0°$; while for a perfectly elastic one (i.e. complete recovery), $\alpha = 90°$.
Bucaille proposes the following empirical equation to relate α to X:

$$\alpha = \frac{1}{0.00854+0.0043 \cdot X} \tag{7}$$

Equations 6 and 7, together with the experimental measurement of P_d, provide a method to calculate the true contact area, A, and eventually determine H_S. For a more detailed explanation of the application of Pelletier's model, the reader is referred to [15].

3.2. Strain rate dependence

The need for a precise evaluation of E and σ_y is now clear, and motivates the characterization of mechanical properties described above. A non-trivial aspect revolves around the consistency of the strain rates enforced during the different types of tests. For an accurate evaluation of the

X parameter, relevant mechanical properties must be obtained for a strain rate which is comparable with the value characteristic of a scratch test performed at a given sliding speed. This involves a range of strain rates which is a few orders of magnitude larger than those typically enforced during DMA or compression tests. To overcome this issue, two different strategies were adopted in the present work.
The dependency of the yield stress on the strain rate is addressed by the well-known Eyring equation [47]:

$$\frac{\sigma_y}{T} = \frac{2}{V^*}\left(\frac{\Delta H}{T} + 2.303R \cdot log\ \frac{\dot{\varepsilon}_y}{\dot{\varepsilon}_0}\right) \quad (8)$$

V^*, ΔH and $\dot{\varepsilon}_0$ are unknown material parameters, whose determination however is not required in this case. Basically, an Eyring-like dependence of the yield stress versus the applied strain rate was assumed and yield stress data for each material were extrapolated to the desired strain rate, assuming a linear dependency in a semi-log scale.
For the modulus, such a general and widely accepted relationship is not available. The extrapolation of E to high strain rates was then carried out by applying a time-temperature reduction scheme to DMA data. Most polymers behave in what is called a thermo-rheologically simple way: curves of a given viscoelastic property as a function of time (or frequency), obtained at different temperatures, can be superimposed by applying a simple translation in a log-log scale to obtain a so-called master curve (valid at a given reference temperature, T_0). The amount by which each curve needs to be translated at a given temperature to superimpose on the reference one is called shift factor, $a_T^{T_0}$, and once determined it allows translating the master curve at any desired temperature [48]. The physical interpretation of this empirical observation is that the temperature does not alter the deformation mechanisms, but only acts via a change in their kinetics (with phenomena occurring faster at higher temperatures [49]). The non-destructive character of DMA tests allowed their execution at several temperatures, with the aim of superimposing relevant data to build a master curve spanning over several decades [50]; in particular, tests were run at progressively lower temperatures, to explore the high-frequency range well beyond the experimental window provided by the DMA instrument.

4. Results

This section is organized as follows: first, the outcome of the bulk mechanical characterization tests (DMA and quasi-static compression) will be presented, together with the extrapolation to high strain rates discussed in the previous section. Results of the scratch tests will follow, separately for the constant-depth and constant-load modalities.

4.1. Mechanical characterization

Figure 2 shows the results of DMA tests in bending, performed on the four materials at varying testing frequencies and temperatures. The experimental scatter between the three (at least) repetitions performed on each material is more evident for the amorphous polymers in particular, while results for LLDPE are more consistent; this can be justified by considering that the greater availability of LLDPE allowed preparation of ad hoc samples in sufficient numbers, while for the other three materials tests had to be performed on the few samples available. For LLDPE a higher sensitivity to the testing frequency (or strain rate) is also reported.
Individual data curves obtained for each material at the different temperatures were then shifted (in a log-log scale) to superimpose them on a master curve, according to the time-temperature reduction scheme detailed in section 3.2. This process results in the master curves displayed in Figure 3, valid for a reference temperature of 25°C, which coincides with that at which compression and scratch tests were performed.

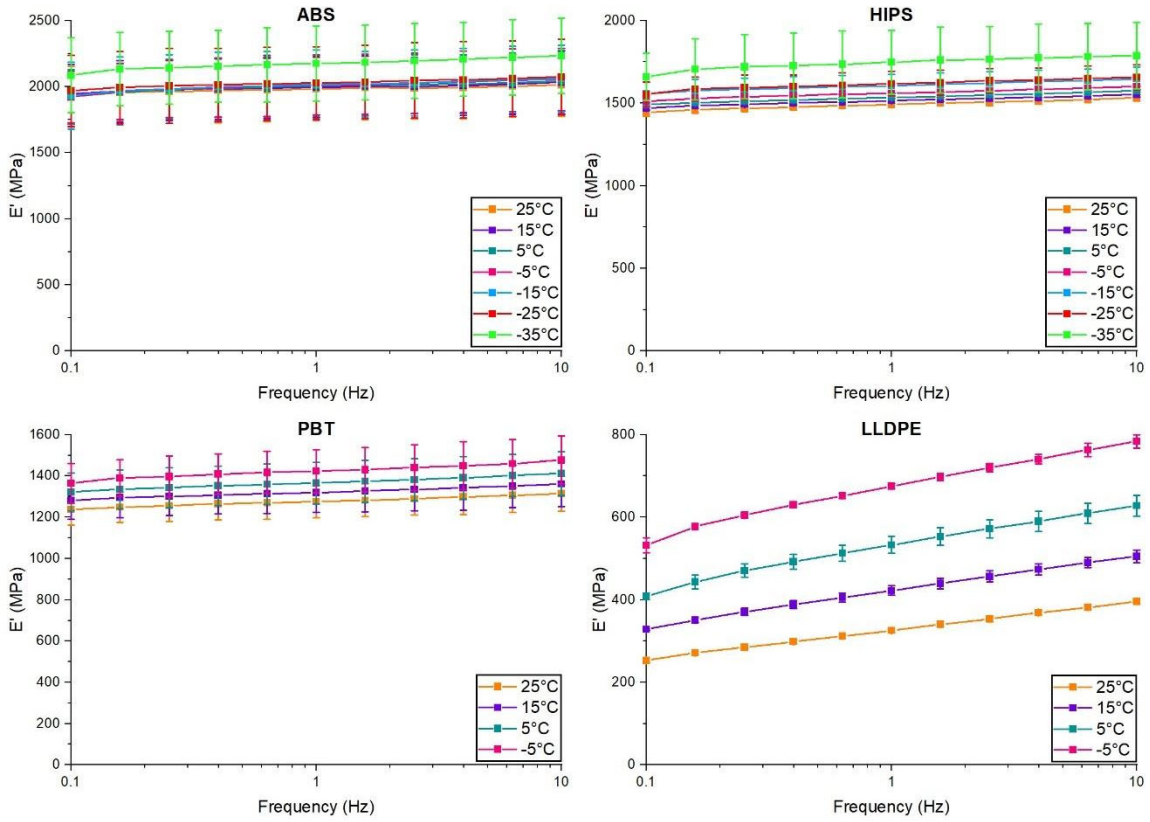

Figure 2. Storage modulus as a function of testing frequency obtained at different testing temperatures; error bars represent the dispersion related to the mean between at least three repetitions (or the standard deviation, in the case of LLDPE).

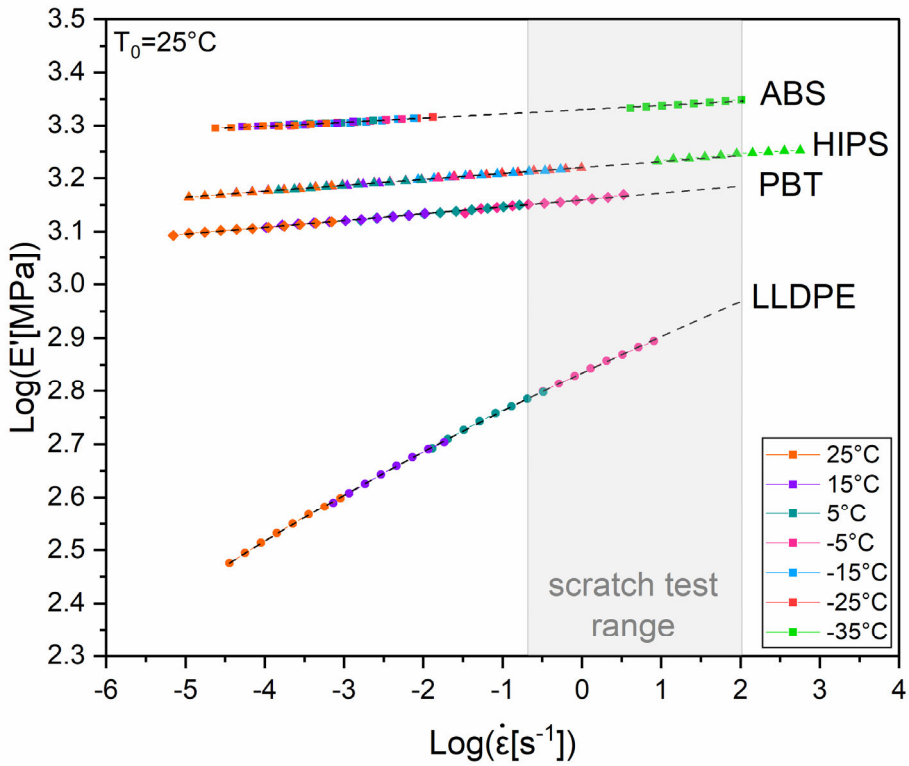

Figure 3. Master curves of the storage modulus at the reference temperature $T_0 = 25°C$ for the four investigated materials. The dashed lines correspond to interpolation of the experimental data, whereas the shaded region represents the strain rate range evaluated for the scratch tests. The effective strain rate was calculated from frequency data according to Equation 1.

The shift factors determined while building the master curves are shown in Figure 4. Values for PBT and LLDPE are almost identical, and also those of HIPS and ABS are quite similar between themselves considering the inherent data dispersion of the measurements and the associated uncertainty in the determination of $a_T^{T_0}$, especially at the lower temperatures.

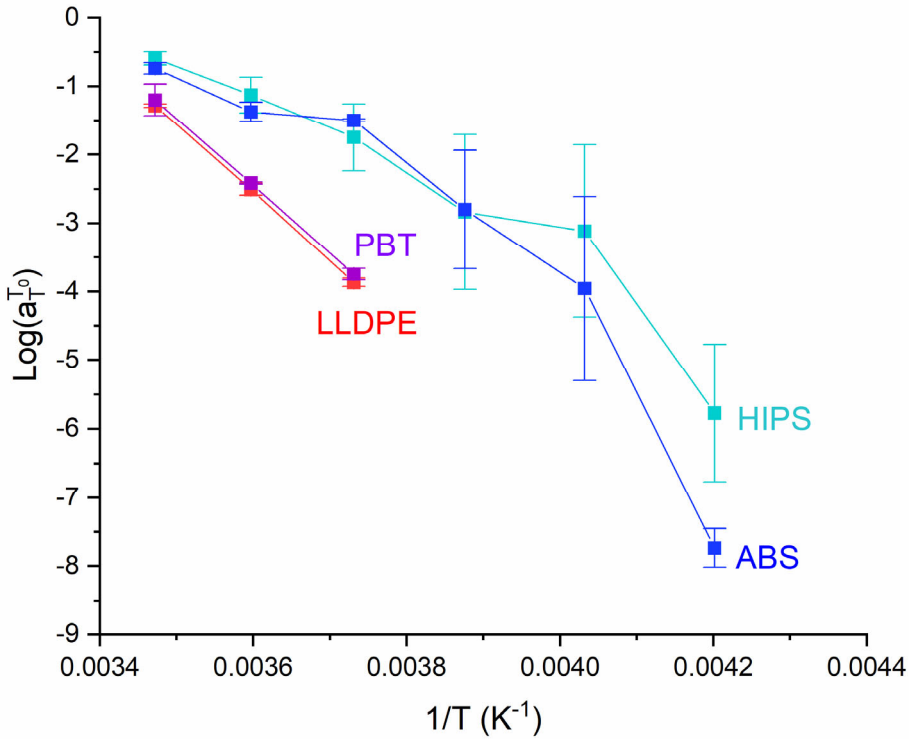

Figure 4. Logarithm of the shift factor as a function of the reciprocal of temperature for the four investigated materials; the error bars represent the error associated to the data dispersion reported in *Figure 2*.

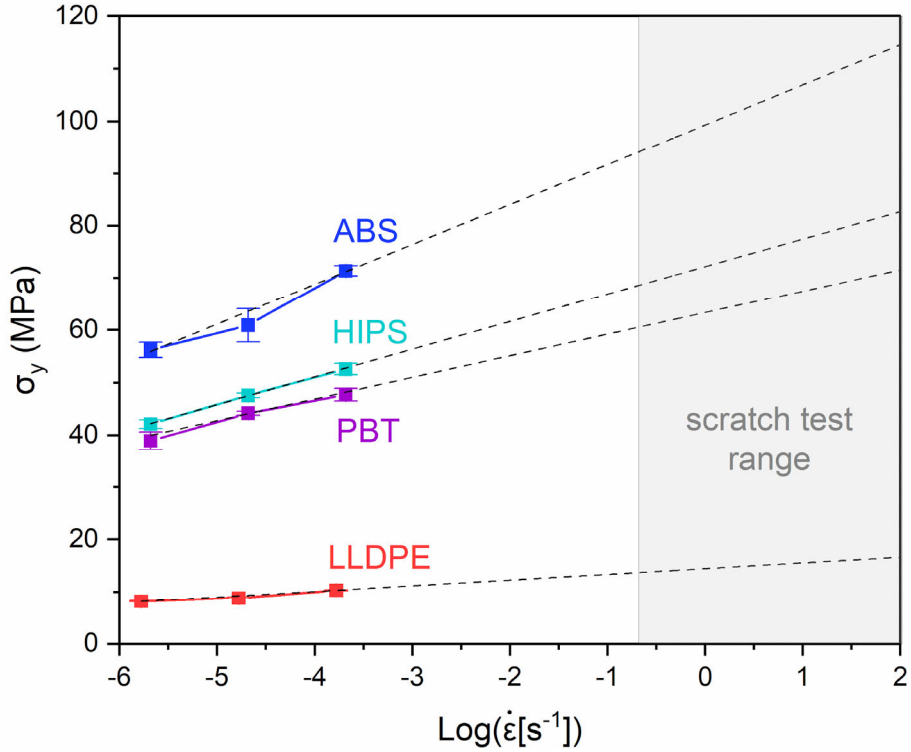

Figure 5. Yield stress vs. strain rate data for the four investigated materials. The dashed lines correspond to a fitting of the data using Eyring's equation (Equation 8), whereas the shaded region represents the strain rate range evaluated for the scratch tests.

Quasi-static compression data, showing the yield stress as a function of the applied strain rate, is displayed in Figure 5. There is some uncertainty in the data for ABS at the intermediate strain rate, probably due to some irregularity in the tested samples. Lack of sufficient material prevented a repetition of the tests, as well as their execution at lower temperatures. Even in the case of yield stress testing at other temperatures would have been of great help, since the experimental values lie well below the effective scratching strain rates; unfortunately, the destructive character of the compression tests performed did not allow for that given the very small number of available samples. The only option was to extrapolate existing data using Eyring's equation (Equation 8), to obtain values whose strain rate was comparable with that of scratch tests.

4.2. Constant depth scratch tests

The typical outputs of a scratch test are the penetration and residual depth (P_d and R_d) corresponding to a given normal load (and possibly the tangential load or friction coefficient, not considered in the present analysis). In the first series of experiments, the chosen approach was a bit different: the normal load, F_N, was instead adjusted (by trial and error, following a preliminary test with ramp load applied) to obtain the same average penetration depth of about 40 μm (±5%) for all the materials and conditions (namely sliding speed). This modality ensures that the scratch geometry is identical for all the tests. As a consequence, the main results of the experiments are the normal load (required to cause the set value of P_d) and R_d. An example is shown for LLDPE in Figure 6.

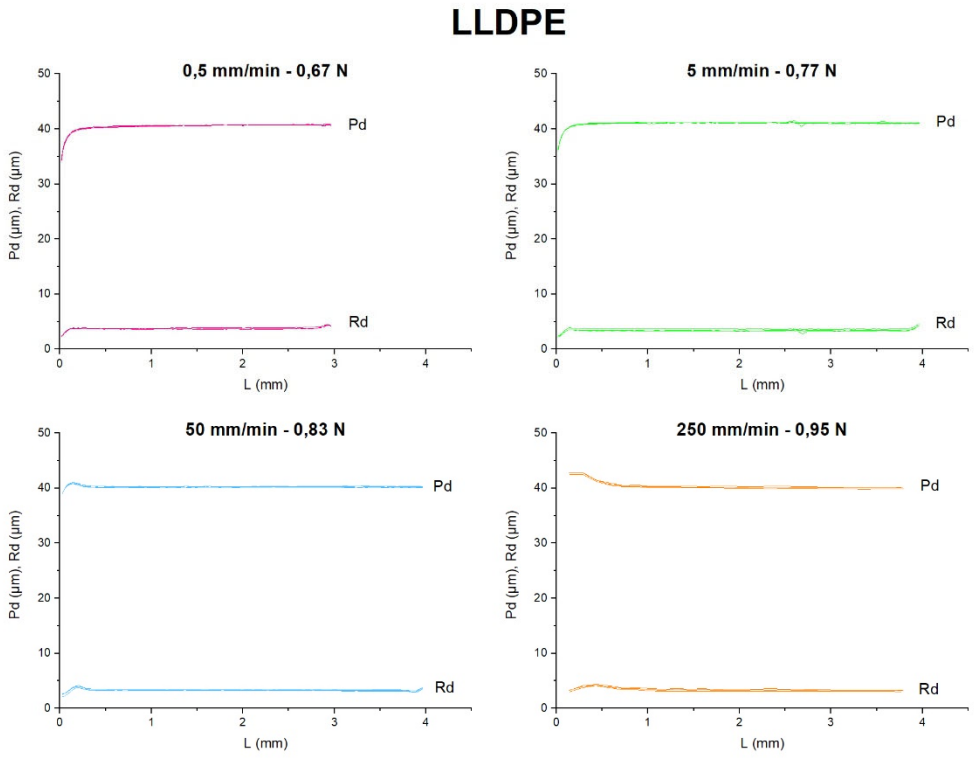

Figure 6. Penetration and residual depths of LLDPE recorded along the scratch length at the four sliding tip velocities, for the 120° indenter. The applied normal load is indicated for each test, corresponding to an average P_d of 40μm.

The results of 3 different scratches are reported in each graph, demonstrating the excellent repeatability of the experimental measurements; the reported behaviour is consistent with the typical ductile ploughing regime. Similar results were obtained for the other materials, except for ABS (and HIPS to a minor extent) which at the lower velocities displayed a certain degree of stick-slip, which introduced some noise in the data, especially at the lowest sliding speeds.
The complete set of values corresponding to the tests performed at 40 μm with the indenter having a 120° apex angle is listed in Table 2, while Figure 7 shows F_N values plotted for each material as a function of the scratch velocity.

Table 2. Results and related parameters of constant depth scratch tests performed using the 120° indenter. For each quantity, average values are reported.

Material	v	F_N	P_d	R_d	$\dot{\varepsilon}$	E	σ_y	$\frac{E}{\sigma_y}$	X	A	H_S
	mm/min	N	μm	μm	s^{-1}	MPa	MPa			mm^2	MPa
HIPS	**0.5**	3.8	40.8	18.7	0.204	1630	68.5	23.8	13.7	0.038	99.1
	5	4.0	38.1	14.4	2.20	2150	102	21.1	13.0	0.035	114
	50	4.5	38.2	14.1	21.7	2190	109	20.0	12.5	0.035	128
	250	5.0	40.8	14.3	104	2220	115	19.4	12.2	0.038	131
ABS	**0.5**	5.3	38.3	14.7	0.218	2110	94.2	22.4	12.9	0.035	149
	5	5.5	38.0	14.3	2.12	2150	102	21.1	12.2	0.035	157
	50	6.0	38.8	14.5	21.7	2190	109	20.0	11.5	0.036	168
	250	6.8	40.1	10.8	104	2220	115	19.4	11.2	0.037	183
RT-PBT	**0.5**	3.3	40.1	9.5	0.208	1410	60.5	23.4	13.5	0.038	87.9
	5	3.5	39.9	8.3	2.09	1460	64.7	22.5	13.0	0.037	94.2
	50	3.8	40.0	8.4	20.9	1500	68.7	21.8	12.6	0.037	102
	250	4.2	41.0	8.7	102	1530	71.6	21.4	12.3	0.038	110
LLDPE	**0.5**	0.67	40.6	3.7	0.205	608	13.8	44.1	25.5	0.040	16.7
	5	0.77	41.1	3.4	2.03	716	14.9	48.2	27.8	0.041	18.8
	50	0.83	40.2	3.3	20.7	834	15.9	52.3	30.2	0.040	20.6
	250	0.95	40.1	3.3	104	920	16.5	55.7	32.1	0.040	23.5

A moderate effect of the sliding velocity is also apparent, with required normal force values becoming progressively higher. This result was expected, since a higher testing speed entails also a higher effective strain rate for a given scratching geometry (fixed in the present case), to which the material responds with increased stiffness and flow stress.
The next, obvious step was to calculate the parameters needed for the application of Pelletier's model. Effective scratch testing strain rates were evaluated according to Equation 2, and the corresponding values of E and σ_y determined taking advantage of the extrapolated data reported in Figure 3 and Figure 5. Relevant values are listed for all velocities in Table 2. Combining the E/σ_y ratio and the indenter geometry through Equation 4, X values can be easily obtained: they are shown in Figure 8. With increasing speed (and strain rate) there is a slight decrease of X, except for LLDPE for which a moderate increase is observed instead; values of LLDPE are also sensibly higher, ranging between 25 and 35 while the other three materials all have very similar X in the 10-15 range.

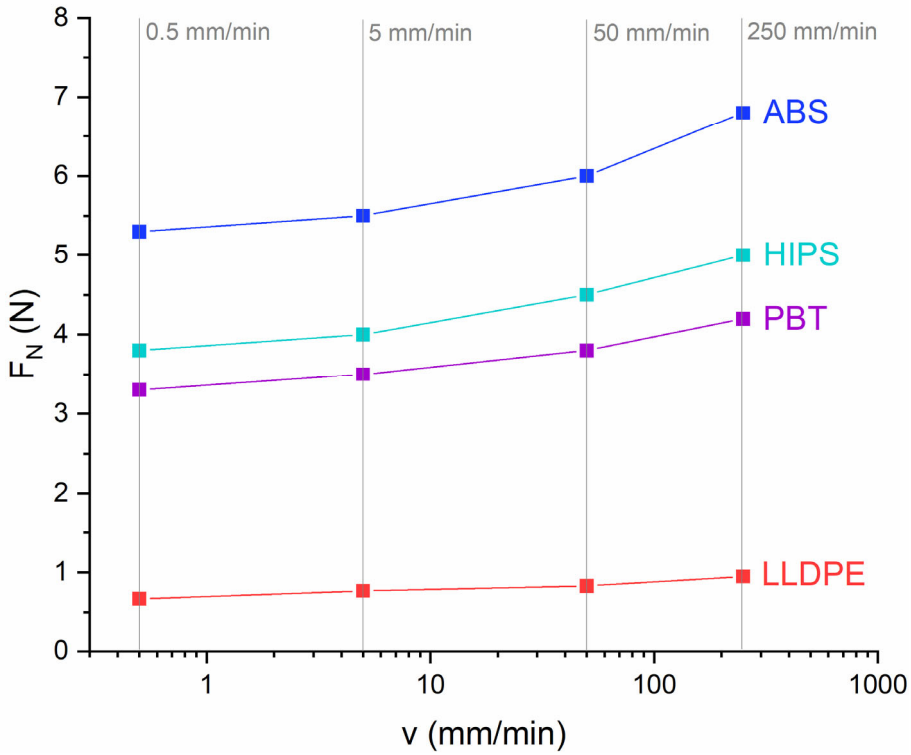

Figure 7. Values of the applied normal forces applied at the four sliding tip velocities in scratch tests at constant depth performed using the 120° indenter.

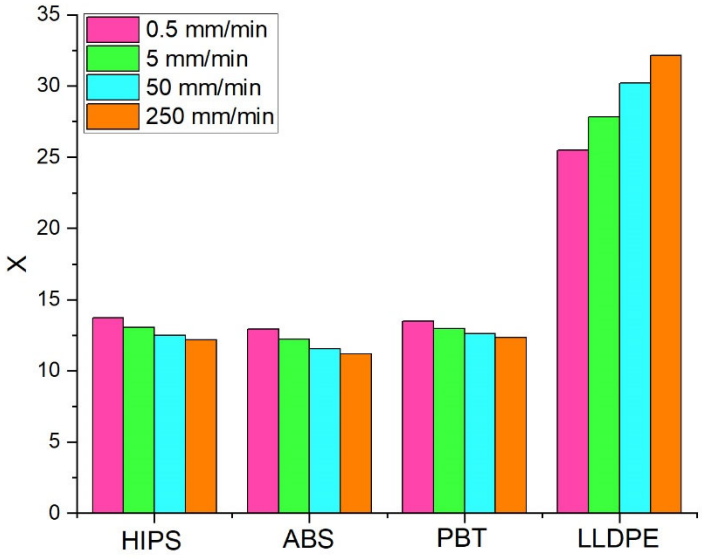

Figure 8. Values of the rheological factor, X, calculated for all the materials at the strain rates corresponding to the scratch velocities used during the constant depth experiments performed with the 120° indenter.

With the X values for all the materials/conditions available, it is quite straightforward to calculate the intermediate parameters c^2 and α using Equations 6 and 7. Since they only depend on the rheological factor, the Pelletier's model predicts similar values for HIPS, ABS and PBT, while a larger c^2 and a smaller α are expected for LLDPE. The first contribution is predominant in the evaluation of the contact area, A, so that a slightly larger value is predicted for LLDPE, as shown in Table 2. Following the determination of A, the scratch hardness, H_S, can finally be

obtained. Relevant values are also listed in Table 2, and plotted as a function of the sliding velocity in Figure 9. Error bars in the graph represent the uncertainty associated to the scatter in the depth data (mentioned before for ABS and HIPS) and to the extrapolation to high strain rate (using 95% confidence bands for the numerical fittings). There is a clear distinction between the levels exhibited by the four investigated materials, as well as a common trend of increasing hardness with increasing sliding speed.

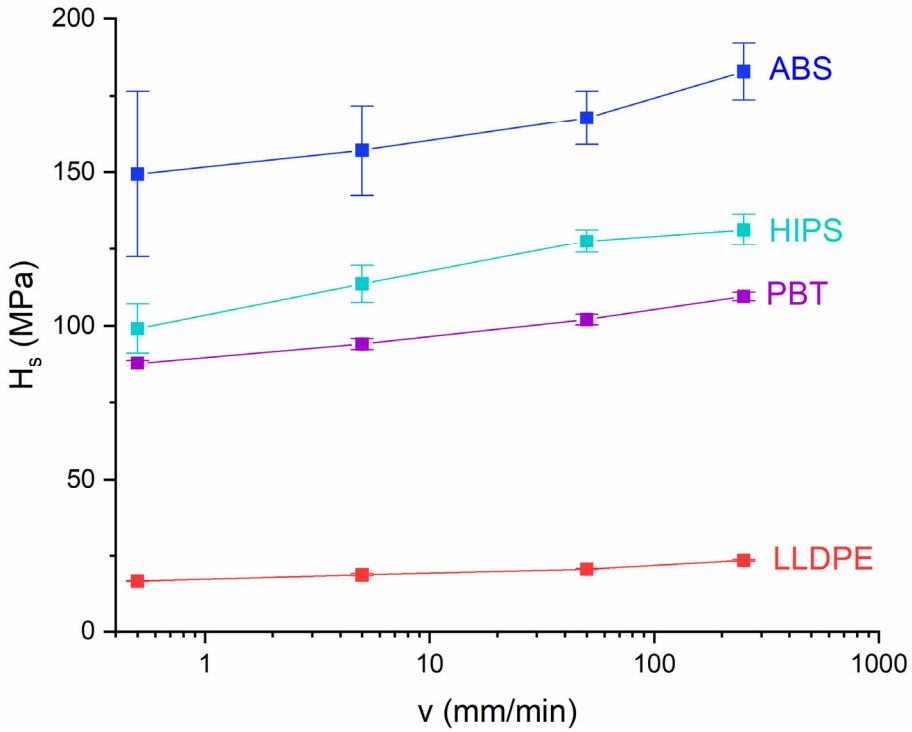

Figure 9. Scratch hardness as a function of sliding velocity for the constant depth test performed using the 120° indenter. Error bars represent the estimated uncertainty of the H_S measurement.

4.3. Constant load scratch tests

To explore the dependence of the identified scratch resistance parameter, H_S, on the applied loading conditions, two additional series of tests were run imposing an identical array of normal loads on the materials under study. Additionally, results were evaluated using two different indenters: the same one used for the constant depth tests, having a 120° apex angle, and a similar sphero-conical indenter with a smaller 90° apex angle. The sharper conical tip results in a more aggressive attack angle, also affecting the value of X via Equation 4.

Table 3 lists the results obtained with the 120° indenter, some of which are the same one previously reported for the same velocity of 50 mm/min. They are presented in detail to allow a comparison with the previously shown constant depth data; similar results were obtained using the 90° indenter. An increasing trend of P_d and R_d with increasing normal load is quite obvious. A comparison between the different materials can be more easily visualized in Figure 10. The most evident result is the significantly higher P_d exhibited by LLDPE, which however is not reflected in R_d data which gives much closer values for the four materials under study – with some differences reported for the two different indenter apex angles. The obvious consequence is that when looking at the relative percentage of recovery, expressed by:

$$recovery = 1 - \frac{R_d}{P_d} \tag{9}$$

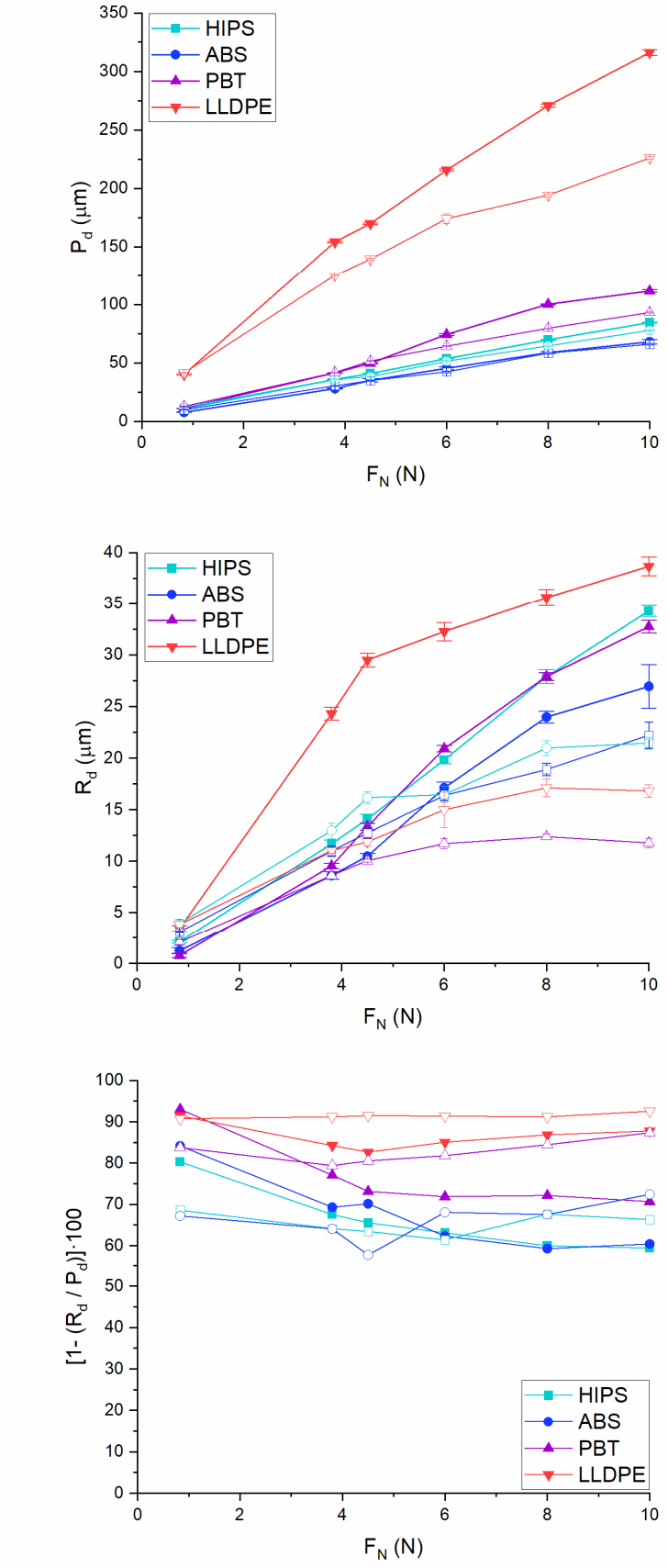

Figure 10. Penetration depth, residual depth and percentage of depth recovery for the constant load scratch tests. Filled symbols: 120° indenter; empty symbols: 90° indenter.

LLDPE displays the highest values, especially with the 90° indenter for which relevant recovery values are always above 90%. In general, no definite trend with the normal load is visible for any of the materials under investigation, except for the lower loads at which the recovery is larger. This finding is consistent with a larger (visco)elastic deformation component expected at lower contact pressures [34].

Table 3. Results and related parameters of constant load scratch tests performed using the 120° indenter at 50 mm/min. For each quantity, average values are reported.

Material	F_N	P_d	R_d	X	A	H_S
	N	μm	μm		mm^2	MPa
HIPS	**0.83**	12.0	3.94	7.37	0.011	74.1
	3.8	36.1	13.0	12.6	0.033	115
	4.5	38.2	14.1	12.6	0.035	128
	6.0	51.5	16.4	12.6	0.051	117
	8.0	64.6	21.0	12.6	0.070	115
	10	77.8	21.4	12.7	0.091	110
0.83	**0.83**	9.90	3.11	5.96	0.009	89.8
	3.8	30.5	11.0	11.5	0.027	138
	4.5	34.8	12.7	11.5	0.032	142
	6.0	38.8	14.5	11.5	0.036	168
	8.0	58.3	18.9	11.6	0.060	133
	10	65.9	22.2	11.7	0.071	141
RT-PBT	**0.83**	12.8	2.08	7.82	0.012	69.6
	3.8	40.0	8.37	12.5	0.037	102
	4.5	51.6	10.1	12.6	0.051	87.7
	6.0	64.2	11.7	12.6	0.069	86.8
	8.0	79.6	12.3	12.7	0.094	84.7
	10	93.1	11.8	12.8	0.120	83.3
LLDPE	**0.83**	40.2	3.27	30.8	0.040	20.6
	3.8	125	11.0	29.4	0.222	17.2
	4.5	139	11.9	29.2	0.266	17.0
	6.0	174	15.0	29.4	0.392	15.3
	8.0	197	18.2	29.1	0.488	16.4
	10	226	16.8	28.8	0.624	16.0

It is useful to plot scratch hardness values as a function of the applied normal load, for the two different indenters; data is reported in Figure 11. Aside from minor differences between the 120° and 90° indenters at high loads (especially for ABS and HIPS), a fairly constant value of H_S can be identified for each material. The most significant deviation is represented by data at the lowest load (0.83 N), for which the scratch hardness values reported for all materials but LLDPE are significantly lower. These aspects will be further explored in the following section.

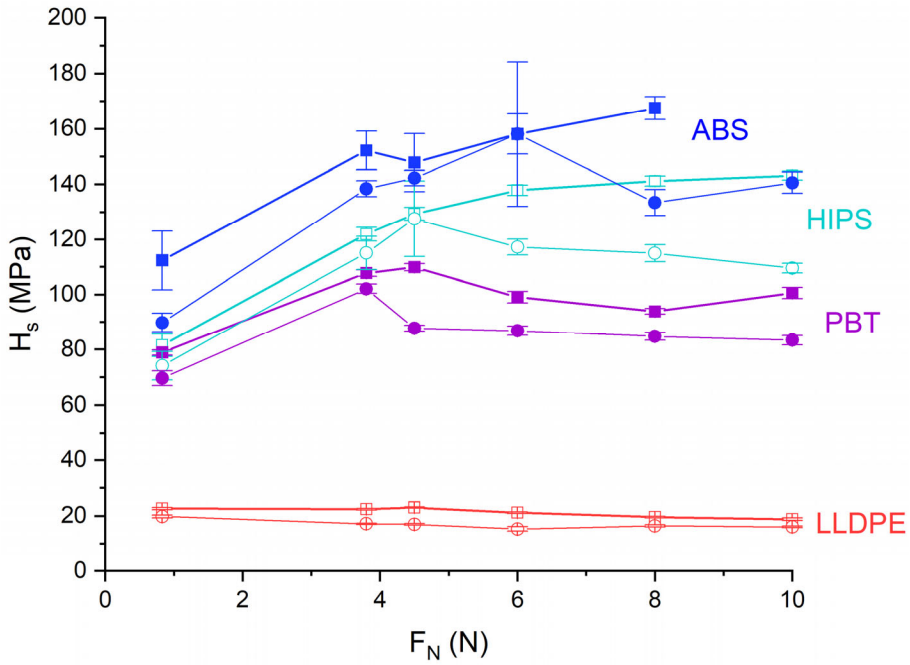

Figure 11. Scratch hardness as a function of normal load for the constant load test performed using the 90° indenter (squares) and 120° indenter (circles). Error bars represent the estimated uncertainty of the H_S measurement.

Discussion

In the works by Kurkcu et al. [15-16], a strong correlation between the scratch hardness and the compressive yield stress was proposed. With reference to the presently investigated materials, the existence of such a correlation is confirmed and strengthened by tests performed at constant penetration depth. The data reported in Figure 12, while consistent with the general trend previously reported by Kurkcu et al. (also plotted for comparison), is remarkably well described by a linear relationship (R^2=0.999) between H_S and σ_y, described by the following equation:

$$H_S = 1.54 \cdot \sigma_y \tag{10}$$

Indeed, the compressive yield stress (evaluated for the correct strain rate) appears to be the controlling factor for scratch hardness, irrespective of the material, applied normal load or sliding velocity.

The difference in hardness between the four materials is quite evident from raw scratch data (as given in Table 2), with LLDPE requiring the lowest load to generate a 40 μm deep scratch, and ABS the highest one. In a similar fashion, P_d values at constant loads (see Table 3) are systematically higher. Such a "hardness", as determined from the purely mechanical quantities measured during a scratch test, is a direct expression of the resistance opposed by a given material to indenter penetration: aspects such as deformation recovery (therefore considering the residual depth of the scratch groove) or scratch visibility are not considered by such an approach.

While Pelletier's model provides a very effective way of calculating scratch hardness values for all the materials, it does not give a completely adequate description of recovery phenomena. This is quite evident from observing R_d values reported in Table 2. Under the low normal loads required to penetrate LLDPE by the desired amount of 40 μm, the material exhibits a very limited amount of plastic deformation (despite its very low hardness). Residual depth for LLDPE remains between 3 and 4 μm; conversely, higher values of R_d (between 10 and 20 μm) were observed on the amorphous polymers, HIPS and ABS, for which a greater amount of plastic yielding occurs because of the higher loads involved (see Figure 14).

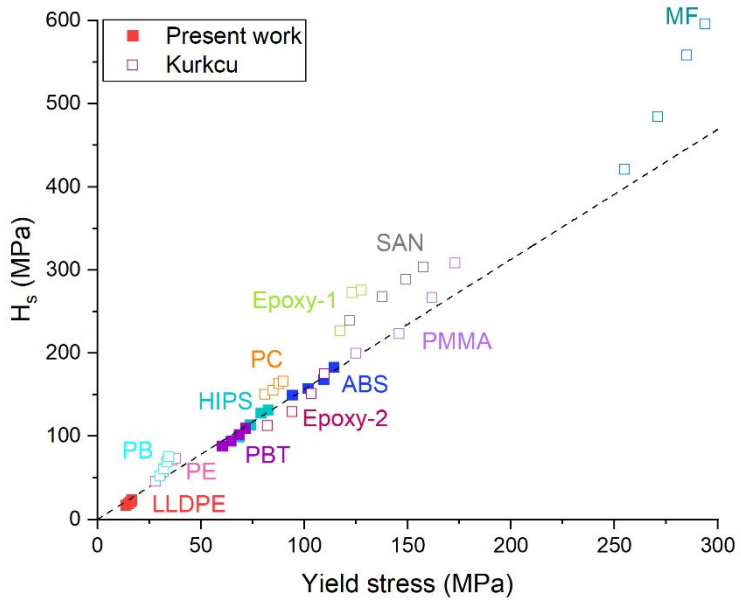

Figure 12. Scratch hardness vs. compressive yield stress for the materials investigated in the present work and in [15-16]. The dashed line represents a linear fit of the data obtained in the present work. All data from constant depth tests performed using an indenter with 120° apex angle.

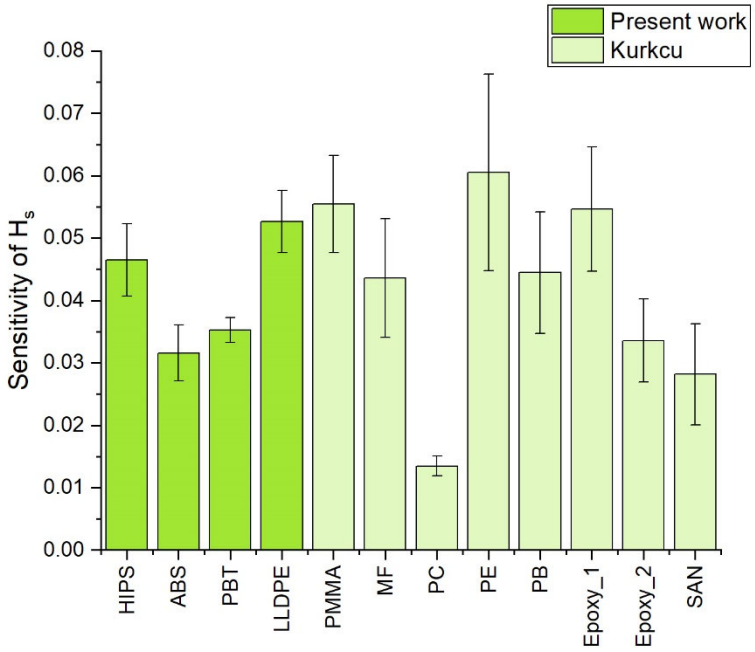

Figure 13. Sensitivity to testing speed of scratch hardness (determined from constant depth tests using a 120° indenter) for the materials investigated in the present work and in [15-16].

Concerning its sensitivity to the sliding speed, a comparison can be drawn between data from the present research and those obtained by Kurkcu et al. on other unfilled polymers [15,16]. A sensitivity parameter can be derived from the average slope of the $\log H_S$ vs. $\log v$ data (shown in linear scale in Figure 9): its values are shown in Figure 13. No particular trend can be identified in view of the structure of the materials involved (whether they are amorphous, semicrystalline, crosslinked) or their characteristic temperatures.

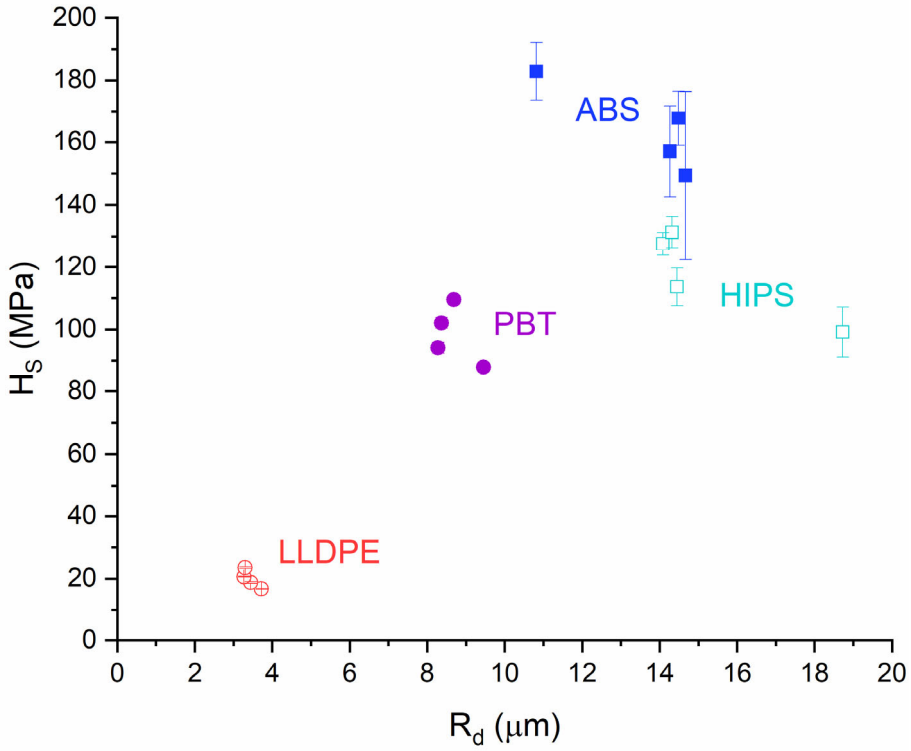

Figure 14. Scratch hardness vs. residual scratch depth from the constant depth tests performed using an indenter with 120° apex angle.

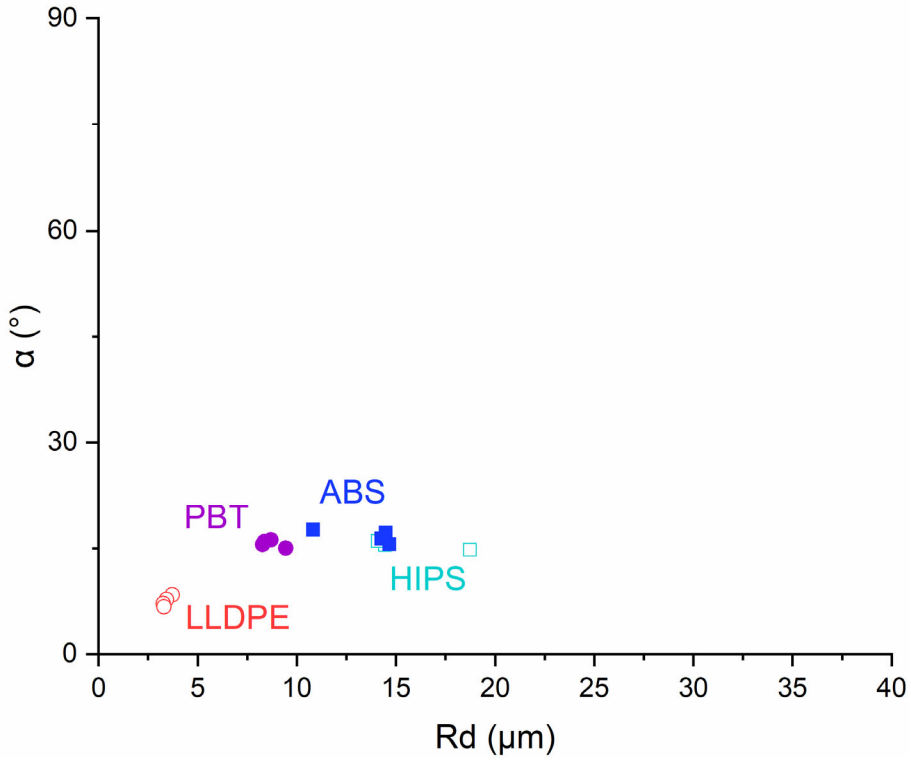

Figure 15. Recovery angle vs. residual scratch depth from the constant depth tests performed using an indenter with 120° apex angle.

This is clearly in contrast with the behaviour which could be expected by considering X values alone. The basic assumption of the model is of an ideally plastic behaviour, with a more pronounced plastic character for materials having a higher X. A direct consequence would be a more "plastic" character for LLDPE, contradicted by the experiments performed with a constant

depth of 40 μm, despite the lower predicted value of α; these results are visible in Figure 15. The model neglects important aspects related to the (visco)elastic contribution to the total deformation, which may become important depending on the applied loading conditions.
The present data can be represented in view of the analysis provided by Lafaye for polymethylmethacrylate (PMMA). In [34], thanks to a scratch apparatus equipped with a built-in microscope, Lafaye was able to analyse the groove left on the scratched surface and associate critical values of the normalised pressure to the boundaries of different behavioural domains, corresponding to elastic, elasto-plastic or plastic contact. The ratio H_S/σ_y was then plotted as a function of the effective strain applied during scratch testing, ε. Lafaye gives the following two alternative expressions for ε:

$$\varepsilon = 0.2\frac{a}{R} \tag{11}$$

$$\varepsilon = 0.2\tan\beta \tag{12}$$

where a, R and β are the contact radius, the tip radius and the attack angle, respectively. Equation 11 is valid when contact occurs on the spherical tip surface, while Equation 12 can be used when the penetration depth is large enough to assume that the main contact surface is the conical one.
The results of experiments performed by Lafaye with different indenters at various temperatures collapse onto a single curve, plotted in Figure 16. Three regions can be identified:

- $H_S/\sigma_y < 1$, where the material behaviour is predominantly elastic
- $H_S/\sigma_y > 1.5$, where the material behaviour is predominantly plastic
- $1 < H_S/\sigma_y < 1.5$, where the material behaviour is elasto-plastic

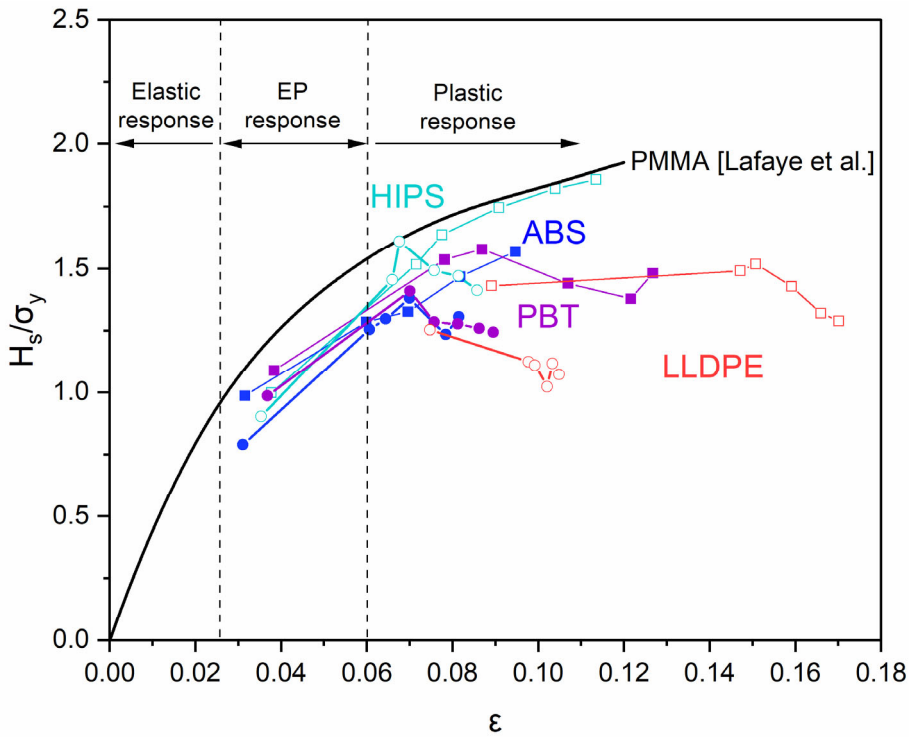

Figure 16. Ratio of scratch hardness over yield stress vs. effective strain for the constant load test performed using the 90° indenter (squares) and 120° indenter (circles). The continuous line represents an interpolation of data reported in [34].

It is quite interesting to compare these results with those from the present work, also reported in the graph. Data for HIPS and ABS lie reasonably close to PMMA (also an amorphous polymer), while those for PBT and especially LLDPE display sensibly lower values, in

particular at high strains. All data points fall in the strain region where PMMA gives a predominantly plastic response, except for the ones obtained under a constant load of 0.83 N, for which on all materials but LLDPE lower scratch hardness values were already pointed out in the comment to Figure 11. The presence of a non-negligible (visco)elastic component of the scratch deformation can explain the apparent reduction of hardness, evaluated according to the procedure described in section 3.1. It is also consistent with the larger amount of recovery already highlighted with reference to the data at the lowest normal load presented in Figure 10. LLDPE data fall completely within the plastic region, with values fairly constant with increasing load/strain, but a marked difference between the two indenters (90° and 120°). It must be noted, however, that in the case of LLDPE the ratio H_S/σ_y involves two quantities which are quite small (compared to the other three materials) and thus more affected by experimental uncertainties and errors. Nevertheless, within this framework there are no elements to justify the larger amount of recovery exhibited by LLDPE (see again Figure 10).
It must be concluded that the approach based on scratch hardness, calculated in the present case through the application of the Pelletier's model, is of limited use if one is interested in evaluation of the post-scratch quality of the surface. Scratch hardness tells only part of the story, being unable to include any information on the important recovery characteristics exhibited by different polymeric materials.

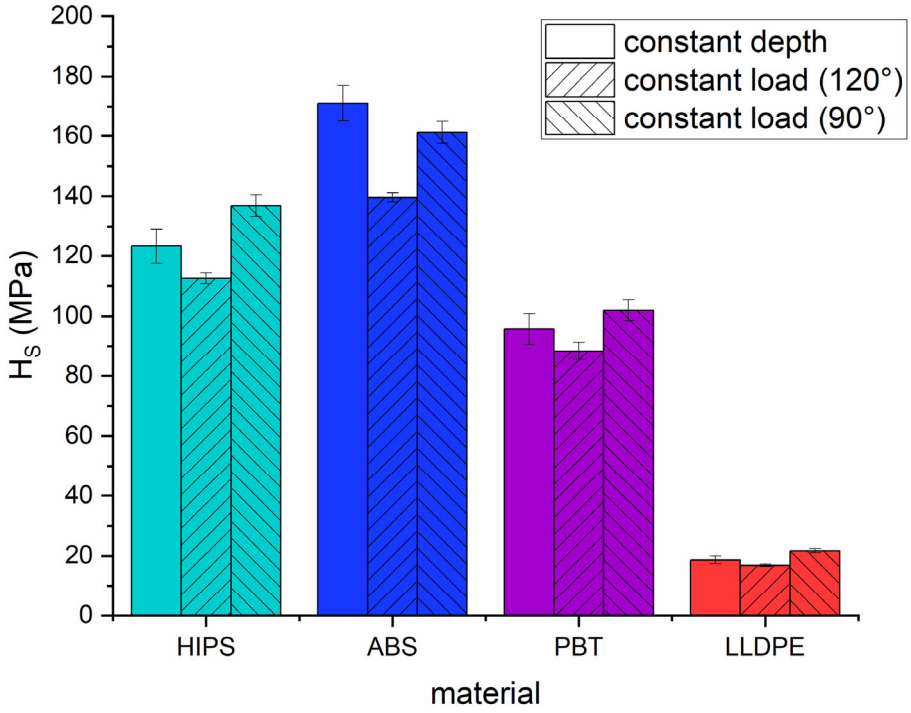

Figure 17. Average scratch hardness evaluated for each testing method and material.

Nevertheless, H_S still provides a reliable indication of the ability of a given material to resist indenter penetration, which is surely related to scratch resistance and can be taken as a direct measurement of it – all the rest being equal (in particular for materials having similar recovery characteristics). Figure 17 collects all hardness valued plotted in Figure 9 and Figure 11, averaged according to the testing condition (constant depth, constant load with 120° indenter and constant load with 90° indenter). For the purpose of this very broad comparison, the dependence of H_S on the sliding velocity has been neglected. Data reported in Figure 17 are weighted averages (with weights and the related error evaluated considering the actual data dispersion). While some differences are clearly present within the data for the individual materials, these are within 20% in the worst case (ABS, for which values were affected by

significant dispersion of the data). Scratch hardness, evaluated according to the proposed procedure, still allows a clear distinction of the performance of the four investigated polymers, irrespective of the testing method considered. H_S can therefore be taken as a quasi-intrinsic (i.e. independent of the loading conditions) parameter to evaluate scratch resistance and rank different materials on absolute terms. Moreover, according to the analysis presented at the beginning of this section, its value can be easily predicted once the compressive yield stress of said materials is known.
The validity of these important results is obviously limited to the (quite common, for polymers) case of materials exhibiting a ductile ploughing scratching mechanism. In presence of very brittle materials (e.g. polymers which suffered degradation, [38]), or of severe testing conditions promoting material cracking and failure, the significance of H_S as a parameter able to describe the scratching process is greatly reduced.
Moreover, the present analysis deals only with the purely mechanical aspects of scratch damage. A clear link between mechanical behaviour and the optical perception of the scratches is still far from being established, although research progressing on both sides (i.e. mechanical and visual) will hopefully succeed in closing this gap. This would be a huge step in the direction of improving how we design and optimize materials (and coatings) in view of their scratch resistance.

Conclusions

This work was aimed at validating a procedure to determine scratch hardness of ductile polymeric materials, i.e. material experiencing ductile ploughing as a consequence of indenter scratching. The important role of the materials' inherent viscoelasticity has been highlighted by the characterization of bulk mechanical properties, which exhibited a marked rate-dependent nature. Recognizing the significant difference between the characteristic time scales of bulk mechanical and scratch testing, relevant properties were extrapolated to the correct strain rate range taking advantage of well-known approaches such as time-temperature superposition (for the elastic modulus) and Eyring's model (for the yield stress). The correct determination of their values was instrumental in the application of the Pelletier's model, which is required to calculate the effective scratch contact area and eventually evaluate scratch hardness.
Scratch hardness is itself a rate-dependent property, due to the viscoelastic character of the polymeric materials under study, although only a mild dependence on the applied sliding velocity was reported in the investigated range of rate (and temperature, which was fixed at room temperature during the scratch experiments).
The limits of such an approach were thoroughly discussed. It is evident that scratch hardness provides a purely mechanical view on the scratch phenomenon, thus neglecting important aspects related to scratch visibility. On the other hand, a clear link between the mechanical performance of polymeric materials and the post-scratch optical quality of their surface is far from being established. Even without exceeding the boundaries of the mechanical aspects, a study of the recovery characteristics of the materials investigated under varying levels of load clarified that scratch hardness describes the response *during* the scratch. This parameter represents the resistance opposed to indenter penetration in the normal direction, and is only partially related to the residual depth of the scratch groove, which is also determined by the viscoelastic recovery of the deformation imposed by the indenter.
Still, provided that the normal force applied is enough to impose a predominantly plastic regime (characteristic of the ductile ploughing scratching mechanism), scratch hardness can be identified as a reliable measure of the scratch resistance: a high value of H_S implies a reduced penetration depth, which can't be but beneficial towards limiting the negative consequences brought by scratch damage. The present work demonstrates how scratch hardness (evaluated

according to the proposed procedure) is relatively independent of the actual loading condition (constant depth or constant load) and indenter shape (varying in terms of the cone attack angle): its value is only mildly influenced by the actual scratch geometry, thus qualifying itself as a good property to rank the performance of different materials, processing parameters and/or conditions. Such a hardness also carries the advantage to be very strongly correlated with the compressive yield stress of the material, irrespective of all testing variables considered (materials, sliding velocity, normal load). A precise evaluation of the material rate-dependence allowed the definition of this correlation in very precise terms, making it a useful tool to predict the behaviour of unknown polymeric materials or the effect that changes in the structural parameters (i.e. crystallinity, orientation, physical ageing) can have on their scratch performance.

Acknowledgements

The authors wish to thank: Prof. Francesco Baldi for supplying the materials to be tested and providing relevant basic mechanical data; Dr. Marco Contino and Mr. Oscar Bressan for their support in sample preparation and setup of the compression tests; Dr. Lorenzo De Noni and Dr. Stefano Tagliabue for helping with the setup of the scratch and DMA tests, respectively; Prof. Andrea Pavan and Prof. Francesco Briatico for the pleasant and fruitful scientific discussions.

References

1. J.S.S. Wong and H.J. Sue, *Scratch behavior of polymers*, Encyclopedia of Polymer Science and Technology, 3rd Ed., Vol. 11, John Wiley and Sons, 2004.
2. C. Xiang, H.J. Sue, J. Chu, B. Coleman, *Scratch behavior and material property relationship in polymers*, Journal of Polymer Science, Part B: Polymer physics, Vol. 39, pp. 47-59, 2001.
3. H. Jiang, R. Browning, H.J. Sue, *Understanding of scratch-induced damage mechanisms in polymers*, Polymer, Vol. 50, pp. 4056-4065, 2009.
4. R.S. Hadal, R.D.K. Misra, *Scratch deformation behavior of thermoplastic materials with significant differences in ductility*, Materials Science and Engineering, 398, pp. 252-261, 2005.
5. L.C.A. van Breemen, L.E. Govaert, H.E.H. Meijer, *Scratching polycarbonate: A quantitative model*, Wear, Vol. 274– 275, pp. 238-247, 2012.
6. B.J. Briscoe and S.K. Sinha, *Scratch resistance and localised damage characteristics of polymer surfaces – A review*, Materialwissenschaft und Werkstofftechnik, Vol. 34(10-11), pp. 989-1002, 2003.
7. B.J. Briscoe, P.D. Evans, E. Pelillo, S.K. Sinha, *Scratching maps for polymers*, Wear, Vol. 200, pp. 137-147, 1996.
8. A. Krupička, M. Johansson, A. Hult. *Use and interpretation of scratch tests on ductile polymer coatings*, Progress in Organic Coatings, Vol. 46, pp. 32-48, 2003.
9. V. Jardret, H. Zahouani, J.L. Loubet, T.G. Mathia, *Understanding and quantification of elastic and plastic deformation during a scratch test*, Wear, Vol. 218, pp. 8-14, 1998.
10. C. Gauthier and R. Schirrer, *Time and temperature dependence of the scratch properties of poly(methylmethacrylate) surfaces*, Journal of Materials Science, Vol. 35, pp. 2121-2130, 2000.
11. Y. Hara, T. Mori, T. Fujitani, *Relationship between viscoelasticity and scratch morphology of coating films*, Progress in Organic Coatings, Vol. 40, pp. 39-47, 2000.
12. G. Kermouche, N. Aleksy, J.M. Bergheau, *Viscoelastic-viscoplastic modelling of the scratch response of PMMA*, Advances in Materials Science and Engineering, 2013.

13. H. Pelletier, C. Mendibide, A. Riche, *Mechanical characterization of polymeric films using depth-sensing instrument: Correlation between viscoelastic-plastic properties and scratch resistance*, Progress in Organic Coatings, Vol. 62, pp. 162-178, 2008.
14. V. Jardret, P. Morel, *Viscoelastic effects on the scratch resistance of polymers: relationship between mechanical properties and scratch properties at various temperatures*, Progress in Organic Coatings, Vol. 48, pp. 322-331, 2003.
15. P. Kurkcu, L. Andena, A. Pavan, *An experimental investigation of the scratch behaviour of polymers: 1. Influence of rate-dependent bulk mechanical properties*, Wear, Vol. 290-291, pp. 86-93, 2012.
16. P. Kurkcu, L. Andena, A. Pavan, *An experimental investigation of the scratch behaviour of polymers: 2. Influence of hard or soft fillers*, Wear, Vol. 317, pp. 277-290, 2014.
17. J. Germann, T. Bensing, M. Moneke, *Correlation between Scratch Behavior and Tensile Properties in Injection Molded and Extruded Polymers*, Polymers, Vol. 14, 1016, 2022.
18. M. Hamdi, H.J. Sue, *Effect of color, gloss, and surface texture perception on scratch and mar visibility in polymers*, Materials & Design, Vol. 83, pp. 528-535, 2015.
19. H. Jiang, R.L. Browning, M.M. Hossain, H.J. Sue, M. Fujiwara*, Quantitative evaluation of scratch visibility resistance of polymers,* Applied Surface Science, Vol. 256, pp. 6324–6329, 2010.
20. C.J. Barr, L. Wang, J.K. Coffey, F. Daver. *Influence of surface texturing on scratch/mar visibility for polymeric materials: a review*, Journal of Material Science, Vol. 52, pp. 1221-1234, 2017.
21. C.J. Barr, L. Wang, J.K. Coffey, A. Gidley, F. Daver. *New technique for the quantification of scratch visibility on polymeric textured surfaces*, Wear, Vol. 384-385, pp. 84-94, 2017.
22. B.J. Briscoe, E. Pelillo, S.K. Sinha. *Characterisation of the Scratch Deformation Mechanisms for Poly(methylmethacrylate) using Surface Optical Reflectivity*, Polymer International, Vol. 43, pp. 359-367, 1997.
23. J. Chrisman, S. Xiao, M. Hamdi, H. Pham, M.J. Mullins, H. Sue, *Testing and evaluation of mar visibility resistance for polymer films*, Polymer Testing, Vol. 69, pp. 238-244, 2018.
24. S. Du, M. Hamdi, H.J. Sue, *Experimental and FEM analysis of mar behavior on amorphous polymers*, Wear, Vol. 444.445, 203155, 2020.
25. P. Gamonal-Repiso, M. Sánchez-Soto, S. Santos-Pinto, M.L. Maspoch, *Influence of topography on the scratch and mar visibility resistance of randomly micro-textured surfaces*, Wear, Vol. 440-441, 203082, 2019.
26. M.M. Hossain, H. Jiang, H. Sue, *Effect of constitutive behavior on scratch visibility resistance of polymers—A finite element method parametric study*, Wear, Vol. 270, pp. 751-759, 2011.
27. A. Dasari, Z.Z. Yu, Y.W. Mai, *Fundamental aspects and recent progress on wear/scratch damage in polymer nanocomposites*, Material Science and Engineering, Vol. R63, pp 31–80, 2009.
28. B.J. Briscoe, P.D. Evans, E. Pelillo, S.K. Sinha, *Scratch hardness and deformation maps for polycarbonate and polyethylene*, B.J.Briscoe, Polymer Engineering and Science, Vol. 36, pp .2996-3005, 1996.
29. V. Le Houérou, C. Robert, C. Gauthier, R. Schirrer. *Mechanisms of blistering and chipping of a scratch-resistant coating*, Wear, Vol. 265, pp. 507-515, 2008.
30. L.P. Sung, P.L. Drzal, M.R. VanLandingham, T.Y. Wu, S.H. Chang, *Metrology for characterizing scratch resistance of polymer coatings*, JCT Research 2, pp. 583–589, 2015.
31. K. Friedrich, H.J. Sue, P. Liu, A.A. Almajid. *Scratch resistance of high performance polymers*, Tribology International, Vol. 44, pp. 1032-1046, 2011.

32. *Standard Test Method for Scratch Hardness of Materials Using a Diamond Stylus*, ASTM G171-03, 2017.
33. C.A. Brookes, P. Green, P.H. Harrison, B. Moxley, *Some observations on scratch and indentation hardness measurements*, Journal of Physics D: Applied Physics, Vol. 5,), pp. 1284-1293, 1972.
34. S. Lafaye, C. Gauthier, R. Schirrer, *Analysis of the apparent friction of polymeric surfaces*, Journal of Materials Science, Vol. 41, pp. 6441–6452, 2006.
35. B.J. Briscoe, P.D. Evans, S.K. Biswas, S.K. Sinha, *The hardness of poly(methylmethacrylate)*, Tribology International, Vol. 29, pp. 93-104, 1996.
36. J.L. Bucaille, E. Felder, G. Hochstetter, *Mechanical analysis of the scratch test on elastic and perfectly plastic materials with the three-dimensional finite element analysis modelling*, Wear, Vol. 249, pp. 422-432, 2001.
37. C. Gauthier, S. Lafaye, R. Schirrer, *Elastic recovery of a scratch in a polymeric surface: experiments and analysis*, Tribology International, Vol. 34, pp. 469-479, 2001.
38. D. Saviello, L. Andena, D. Gastaldi, L. Toniolo, S. Goidanich, *A multi-analytical approach for the morphological, molecular and mechanical characterization after photo-oxidation of polymer used in artworks*, Journal of Applied Polymer Science, Vol. 135, 46194, 2018.
39. L. Andena, S. Tagliabue, A. Pavan, A. Marenghi, M. Testa, R. Frassine, *Probing athletics tracks degradation using a microscratch technique*, Polymer Testing, Vol. 89, , 106602, 2020.
40. M. Freschi, M. Di Virgilio, O. Haiko, M. Mariani, L. Andena, N. Lecis, J. Kömi, G. Dotelli, *Investigation of second phase concentration effects on tribological and electrical properties of Cu-WS2 composites*, Tribology International, Vol. 166, 107357, 2022.
41. M. Freschi, A. Arrigoni, O. Haiko, L. Andena, J. Kömi, C. Castiglioni, G. Dotelli, *Physico-mechanical properties of metal matrix self-lubricating composites reinforced with traditional and nanometric particles*, Lubricants, Vol. 10(3), 35, 2022.
42. F. Baldi, L. Andena, B.R.K. Blackman, L. Castellani, P.M. Frontini, J. Kucera, L. Laiarinandrasana, A. Pegoretti, A. Salazar, L. Warnet, *Determination of the fracture resistance of ductile polymers: the ESIS TC4 recent experience*, Materials Performance and Characterization, Vol. 9 (5), pp. 675-687, 2020.
43. J.L. Bucaille, C. Gauthier, E. Felder, R. Schirrer, *The influence of strain hardening of polymers on the piling-up phenomenon in scratch tests: Experiments and numerical modelling*, Wear, Vol. 260, pp. 803-814, 2006.
44. M .Contino, L. Andena, M. Rink, A. Colombo, G. Marra, *Fracture of high-density polyethylene for bleach bottles*, Procedia Structural Integrity, Vol. 2, pp. 213-220, 2016.
45. M. Contino, L. Andena, M. Rink, G. Marra, S. Resta, *Time-temperature equivalence in environmental stress cracking of high-density polyethylene*, Engineering Fracture Mechanics, Vol. 203, pp. 32-43, 2018.
46. M. Contino, L. Andena, V. La Valle, M. Rink, G. Marra, S. Resta. *A comparison between K and G approaches for a viscoelastic material: the case of environmental stress cracking of HDPE.* Mechanics of Time-Dependent Materials, Vol. 24, pp. 381–394, 2020.
47. M. Contino, L. Andena, M. Rink, *Environmental Stress Cracking of High-Density Polyethylene under plane stress conditions,* Engineering Fracture Mechanics, Vol. 241, 107422, 2021.
48. C. Bauwens-Crowet, J.C. Bauwens, G. Homès, *The temperature dependence of yield of polycarbonate in uniaxial compression and tensile tests*, Journal of Materials Science, Vol. 7, pp.176–183, 1972.
49. R.M. Christensen, *Theory of Viscoelasticity—An Introduction*, Academic Press, New York, 1982.
50. L.E. Nielsen, *Mechanical Properties of Polymers*, Reinhold, New York, 1962.